A Quantitative Model for Allosteric Control of Purine Reduction by Murine Ribonucleotide Reductase†

Charles P. Scott,‡,§ Ossama B. Kashlan,‡ James D. Lear,|| and Barry S. Cooperman*,‡

Department of Chemistry, University of Pennsylvania, Philadelphia, Pennsylvania 19104-6323, and Department of Biochemistry and Biophysics, School of Medicine, University of Pennsylvania, Philadelphia, Pennsylvania

Received October 5, 2000; Revised Manuscript Received December 8, 2000

ABSTRACT: The reduction of purine nucleoside diphosphates by murine ribonucleotide reductase requires catalytic (R1) and free radical-containing (R2) enzyme subunits and deoxynucleoside triphosphate allosteric effectors. A quantitative 16 species model is presented, in which all pertinent equilibrium constants are evaluated, that accounts for the effects of the purine substrates ADP and GDP, the deoxynucleoside triphosphate allosteric effectors dGTP and dTTP, and the dimeric murine R2 subunit on both the quaternary structure of murine R1 subunit and the dependence of holoenzyme ($R1_2R2_2$) activity on substrate and effector concentrations. R1, monomeric in the absence of ligands, dimerizes in the presence of substrate, effectors, or $R2_2$ because each of these ligands binds $R1_2$ with higher affinity than R1 monomer. This leads to apparent positive heterotropic cooperativity between substrate and allosteric effector binding that is not observed when binding to the dimeric protein itself is evaluated. Allosteric activation results from an increase in k_{cat} for substrate reduction upon binding of the correct effector, rather than from heterotropic cooperativity between effector and substrate. Neither the allosteric site nor the active site displays nucleotide base specificity: dissociation constants for dGTP and dTTP are nearly equivalent and K_m and k_{cat} values for both ADP and GDP are similar. $R2_2$ binding to $R1_2$ shows negative heterotropic cooperativity vis-à-vis effectors but positive heterotropic cooperativity vis-à-vis substrates. Binding of allosteric effectors to the holoenzyme shows homotropic cooperativity, suggestive of a conformational change induced by activator binding. This is consistent with kinetic results indicating full dimer activation upon binding a single equivalent of effector per $R1_2R2_2$.

Ribonucleotide reductases (RRs)[1] form a family of allosterically regulated enzymes that catalyze the conversion of ribonucleotides to 2′-deoxyribonucleotides (*1*). As this reaction constitutes the only metabolic pathway for the production of deoxyribose, which is essential for de novo DNA biosynthesis, mammalian RR is an important target for anticancer and antiviral chemotherapeutic agents (*2*−*4*). All known RRs accept the four common ribonucleotides as substrates. Enzymatic activity toward a given nucleotide substrate generally depends on the presence of allosteric effector molecules. For class Ia RRs, which comprise all eucaryotic RRs as well as some from eubacteria, bacteriophages and viruses (*1*), ATP stimulates the reduction of pyrimidine nucleoside diphosphate substrates (*5*), dTTP stimulates the reduction of GDP, dGTP stimulates the reduction of ADP, and dATP serves as a general inhibitor (*6*−*8*). This elaborate regulatory scheme ensures a balanced pool of deoxynucleotide monomers for DNA replication. Mutations affecting the allosteric regulation of RR, for instance by interfering with the ability of RR to discriminate with high specificity between eight chemically similar ligands (four nucleotide substrates and four nucleotide effectors), are deleterious because the resulting aberrant nucleotide pools significantly impact replicative fidelity (*1*, *9*−*11*).

The enzymatic activity of class Ia RRs depends on the formation of a complex between two different subunits, R1 and R2. The R2 subunit contains a stable tyrosyl free radical that is necessary for enzymatic activity (*10*). The enzyme active site, as well as two kinds of allosteric sites, denoted the specificity and activity sites, are located on the R1 subunit. Binding and activity data for several class Ia RRs have been formulated into a phenomenological model (*12*) that provides a valuable qualitative guide for predicting which activity will be manifest under specific conditions. In this model, ATP and dATP can bind to both allosteric sites, while dTTP and dGTP bind only to the specificity site (*13*, *14*). The reduction of specific NDPs by RR depends on the occupancy of these sites. Allosteric effector binding has also been shown to influence the quaternary structure of R1 (*7*, *15*), but this effect has not been considered explicitly in existing phenomenological models of RR actvity.

† Supported by NIH Grants CA58567 (to B.S.C.) and GM07229 (to C.P.S.).

* To whom correspondence should be addressed. Phone: (215) 898-6330. Fax: (215) 898-2037. E-mail: cooprman@pobox.upenn.edu.

‡ Department of Chemistry, University of Pennsylvania.

§ Current address: Department of Chemistry, 152 Davey Laboratory, The Pennsylvania State University, University Park, Pennsylvania 16802.

|| Department of Biochemistry and Biophysics, University of Pennsylvania.

[1] Abbreviations: C, $R1_2R2_2$ complex; DLS, dynamic light scattering; mRR, murine ribonucleotide reductase; mR1, murine ribonucleotide reductase large subunit; mR2 murine ribonucleotide reductase small subunit; PMSF, phenylmethyanesulfonylfluoride; RR, ribonucleotide reductase; R1, ribonucleotide reductase large subunit; R2, ribonucleotide reductase small subunit; SE, sedimentation equilibrium.

10.1021/bi002335z CCC: $20.00
Published on Web 01/17/2001

In no case has a quantitative model been put forward for a class Ia RR that accounts for observed activities in terms of the distribution of specific species in solution and the enzymatic activity of each species. The absence of such a model makes it difficult to achieve full understanding of site-to-site interactions or of mutations affecting activity (since it is not clear which interactions are being affected) or to predict changes in in vivo activity resulting from changes in concentrations of nucleotides or RR subunits. An important part of the problem has been the failure to explicitly consider R1 oligomerization state as a variable influencing ligand binding and RR activity.

Here, and in a related study (O.B.K. et al., manuscript in preparation), we directly address this lack by examining R1 oligomerization, R1 ligand binding, and enzymatic activity under identical conditions as functions of R1, R2, substrate, and effector concentrations. We begin by considering mRR activity toward the purine substrates ADP and GDP. This is a good starting point for the development of a quantitative description of RR activity because reduction of these substrates is fully activated through binding at the specificity site and does not require the presence of either of the activity-site ligands, ATP or dATP. Our results permit formulation of a 16 species model in which all pertinent equilibrium constants are evaluated, allowing quantification of homotropic and heterotropic site-to-site interactions.

EXPERIMENTAL SECTION

Materials. The plasmid pET-M2 (pET3a-R2) encoding the murine R2 subunit was a gift from Dr. Lars Thelander (*16*) and was grown in BL21(DE3) cells. R2 was purified as described (*17*). The gene encoding the large (R1) subunit of murine ribonucleotide reductase was a gift from Dr. Ingrid Caras (Genentech) (*18*). The mouse carboxy-terminal heptamer, FTLDADF, was provided by Dr. Alison Fisher (*19*). Radiolabeled dGTP (2,8-[^{3}H]dGTP) was purchased from New England Nuclear. Radiolabeled dTTP (5-Me-[^{3}H]dTTP) was obtained from ICN. Ultrafree MC filter units (30 000 kDa) were from Millipore. All other materials were of the highest available purity.

Expression and Purification of Recombinant Murine R1. R1 was expressed and purified as described previously (*20*), with the following modifications. High-5 cells (InVitrogen) were used for expression, replacing Sf9 cells. Cells were suspended in 50 mM Tris-HCl, pH 7.6, and 100 μM dithiothreitol (DTT) (buffer A) with added protease inhibitors [2 mM phenylmethanesulfonylfluoride (PMSF) and 1 μM leupeptin and pepstatin] and lysed by two rounds of freeze−thaw (−78 to 37 °C). The crude lysate was centrifuged in a Sorvall SS34 rotor for 20 min (19 000 rpm, 43000*g*) at 4 °C. The supernatant was treated with 10% (w/v) streptomycin sulfate to a final concentration of 2.5%, stirred on ice for 10 min, and centrifuged as above. Solid ammonium sulfate was added to the supernatant (0.586 g/mL, 0−80% saturation) while stirring over 15 min on ice. Stirring was continued for 1 h, and the precipitate was collected by centrifugation as above. The pellet was resuspended in 5−10 mL of buffer A plus protease inhibitors to a final protein concentration of approximately 30 mg/mL. The total volume was loaded onto a Sephadex G-25 column (1.1 cm^2 × 43 cm, 1−2 mL/min) that had been equilibrated with buffer A plus protease inhibitors. Protein containing fractions devoid of ammonium sulfate (approximately 25 mL) were pooled and loaded directly onto a preequilibrated FTLDADF-Sepharose affinity column (*21*) (5 cm^2 x 2 cm, 5 mL/min, 10 mL bed volume). Nonspecifically bound protein was removed from the column with 250 mL of buffer A. Specifically bound protein was eluted with 300 mL of buffer A containing 500 mM KCl. The eluant was concentrated in an Amicon pressure cell with a PM-10 ultrafiltration membrane to a volume of 10−15 mL and dialyzed overnight at 4 °C versus buffer A containing 100 mM KCl. The dialyzed protein was concentrated to approximately 5 mg/mL in an Amicon pressure cell with a PM-30 ultrafiltration membrane (approximately 5−10 mL). The concentrated material was centrifuged to remove any precipitate, quick frozen in liquid nitrogen and stored at −80 °C.

Methods. Determination of Protein and Nucleotide Concentrations. Protein and nucleotide concentrations were determined using the following molar extinction coefficients ($M^{-1}cm^{-1}$): apo-R2 monomer $\epsilon_{280-310} = 62\,000$ (*16*); R1 monomer, $\epsilon_{280-320} = 108\,000$ (*14*, *22*); adenine, $\epsilon_{260} = 15\,000$; guanosine, $\epsilon_{254} = 13\,500$; thymidine, $\epsilon_{268} = 9500$ (*23*). Nucleotides were stored at −20 °C. Both radiolabeled and unlabeled nucleoside triphosphates were monitored for hydrolysis by polyethylene-imine thin-layer chromatography in 2 mM formic acid/0.5 mM LiCl (*24*). Stocks with greater than 10 percent hydrolysis were discarded.

Dynamic Light Scattering. Dynamic light-scattering measurements on the R1 subunit were made with a DynaPro-801 dynamic light-scattering instrument (Protein Solutions) at ambient temperature (19.4−24.8 °C). Measurements were made in 50 mM hydroxyethylpiperazine-ethanesulfonic acid (HEPES), pH 7.6, 25 mM DTT, 10 mM KCl, 10 mM $MgCl_2$, and 7 mM NaF (buffer B) with R1 and ligand (effector and/or substrate) concentrations as indicated. Samples were filtered through 0.1 μm Anotop-10 (Whatman) filters to remove dust and particulate matter. In a typical experiment, 100−200 μg of R1 and increasing amounts of ligand were combined in a final volume of 200 μL of buffer B and incubated at ambient temperature for 5 min prior to injection into the instrument.

Nucleotide Binding Assays. Binding of ligands to R1 or the R1−R2 complex was measured by the method of Ormö and Sjöberg (*25*) with the following modifications. Each assay contained buffer B plus 50 μM $FeCl_3$, R1, R2, substrate, and radiolabeled effector, as indicated, in a total volume of 150 μL. Reaction mixtures containing all components except effector in a volume of 120 μL were incubated at 25 °C for 5 min in the upper reservoir of an Ultrafree MC filter unit prior to initiation with 30 μL of radiolabeled effector. A 30 μL aliquot of the complete assay mixture was removed to measure the total ligand concentration in the assay. Complete reaction mixtures were then incubated at 25 °C for 5 min, and centrifuged at 6000*g* for 30−120 s, until 25−75% of the volume in the upper reservoir was passed through the ultrafiltration membrane. Radioactivity in free and total ligand aliquots was quantified by liquid scintillation counting.

Analytical Ultracentrifugation. Analytical ultracentrifugation studies were carried out using a Beckman Optima XL-I analytical ultracentrifuge equipped with Rayleigh interference optics and an An60-Ti rotor. Samples were made

up in buffer C (50 mM Tris-HCl, pH 7.6, 10 mM KCl, 10 mM $MgCl_2$, 25 mM β-mercaptoethanol, and 7 mM NaF). 50 μM $FeCl_3$ was added to the buffer in samples containing R2.

Sedimentation Velocity. Samples were placed into an aluminum Epon synthetic boundary cell. Centrifugation was carried out at 25 °C at 40 000−48 000 rpm. Interference fringe displacement data was collected as often as possible until the boundary reached the end of the cell. Data scans to be analyzed were selected with the aid of data movies created using a macro program for Igor Pro. Analysis was performed with the program DCDT (*26*−*28*), which converts differences in concentration profiles of scans as functions of r and t into a $g(s^*)$ vs s^* curve, where $g(s^*)$ is the distribution of apparent sedimentation coefficients, denoted s^*. When macromolecular components do not interact on the time scale of the experiment, the resulting $g(s^*)$ vs s^* curve for each component is essentially Gaussian, with the maximum value of $g(s^*)$ occurring at s^* equal to s, the true sedimentation coefficient. When components interact to form a complex, as in the case of R1 and R2, the maximum value of $g(s^*)$ occurs at an s^* value intermediate between the s value for the complex and the higher of the component s values, with the exact position dependent on component concentration and the equilibrium constant for complex formation.

Calculated s values were determined from eq I (*29*)

$$S_{calc} = {}^1/_3[(1 - \nabla\rho)/\eta][M/N_o\pi\tau]^{2/3}[{}^1/_6\nabla]^{1/3} \qquad \text{(I)}$$

in which M is molecular mass, N_0 is Avogadro's number, η is the intrinsic viscosity of the solution [1.13 g/ms, calculated using SEDNTERP (John Philo, http://www.cauma.uthsc-sa.edu/software/)], ∇ is the partial specific volume [0.73 cm^3/g], and ρ is the buffer density.

Sedimentation Equilibrium. Samples were centrifuged for times sufficient to achieve equilibrium in three-compartment carbon-epoxy centerpieces using sapphire windows. Data obtained by interference fringe displacement was analyzed by nonlinear least-squares curve-fitting of radial concentration profiles using the Marquardt−Levenberg algorithm implemented in Igor Pro (Wavemetrics, Oswego, OR) with a user-defined function coding eq II (*30*),

$$n(r) = \text{baseline} + \sum_i iM_w \frac{dn/dc}{\lambda} l \frac{C_o^{\,i}}{K_i} \exp\left\{ iM_w \frac{(1 - \bar{v}\rho)\omega^2}{2RT}(r^2 - r_o^{\,2}) \right\} \qquad \text{(II)}$$

describing n reversible associations in centrifugation, in which $n(r)$ is the number of fringes due to all sedimenting species ($i = 1, 2, ..., i$) at radial position r. Here, $K_i = i$-mer dissociation constant [$M^{(i-1)}$], dn/dc = refractive increment [0.187×10^{-3} fringes L/g (*31*)], $\lambda = 675$ nm, l = path length (1.2 cm), M_w = monomer molecular weight of sedimenting species (90 000 g/mol), r_o = arbitrary fixed radius reference, C_o = molar concentration at r_o of monomer of molecular weight, M_w, ω = angular velocity of rotor (rad/s), and υ and ρ are as defined above. In examining R1 dimerization, two data sets were fit simultaneously with the dissociation constant as the global fitting parameter. Baseline and C_o values for each data set were allowed to vary independently in fitting.

Table 1: Definitions of Equilibrium Constants[a]

equilibrium constant	definition
K_o	$= [R1]^2/[R1_2]$
K_o^L	$= [R1L]^2/[R1_2L_2]$
K_o^S	$= [R1S]^2/[R1_2S_2]$
K_S	$= 2[R1_2][S]/[R1_2S] = 0.5[R1_2S][S]/[R1_2S_2]$
K'_S	$= [R1][S]/[R1S]$
K_L	$= 2[R1_2][L]/[R1_2L] = 0.5[R1_2L][L]/[R1_2L_2]$
K'_L	$= [R1]\,[L]/[R1L]$
K_C	$= [R1_2][R2_2]/[R1_2R2_2] = [R1_2][R2_2]/[C]$
K'_C	$= [R1][R2_2]/[R_1R2_2]$
K_L^S	$= 2[R1_2S_2][L]/[R1_2LS_2] = 0.5[R1_2LS_2][L]/[R1_2L_2S_2]$
$K_{L,1}^C$	$= [C][L]/[CL]$
$K_{L,2}^C$	$= [CL][L]/[CL_2]$
$K_L^{C,S}$	$= 2[CS_2][L]/[CLS_2] = 0.5[CLS_2][L]/[CL_2S_2]$
K_C^L	$= [R1_2L_2][R2_2]/[C_{L2}]$
$K_C^{L,S}$	$= [R1_2L_2S_2][R2_2]/[CL_2S_2]$
K_C^S	$= [R1_2S_2][R2_2]/[CS_2]$
K_S^L	$= 2[R1_2L_2][S]/[R_{12}L_2S] = 0.5[R1_2L_2S][S]/[R1_2L_2S_2]$
K_S^C	$= 2[C][S]/[CS] = 0.5[CS][S]/[CS_2]$
K_m	$= 2[CL_2][S]/[CL_2S] = 0.5[CL_2S][S]/[CL_2S_2]$

[a] C is the $R1_2R2_2$ complex.

Activity Assays. Ribonucleotide reductase activity was assayed under initial rate conditions at 25 °C as described (*8*), with minor modifications. Each assay contained buffer B with 50 μM $FeCl_3$ and R1, R2, effector and radiolabeled substrate, as indicated, in a volume of 100 μL. Reactions were initiated with radiolabeled substrate and quenched by immersion in a boiling water bath for four min. Tritiated samples were frozen and lyophilized to dryness to reduce backgrounds. Lyophilized samples were reconstituted in 1 mL of 50 mM Tris-HCl, pH 8.5, with 100 mM $Mg(OAc)_2$ (buffer D) and centrifuged at 6000*g* for 10 min in a microfuge to remove denatured protein. Reconstituted samples were loaded onto phenylboronate-agarose columns (Amicon, 2 mL bed volume), preequilibrated with 15 mL of buffer D. Purine deoxyribonucleoside diphosphates elute in 8 mL of buffer D. Unreacted ribonucleoside diphosphate substrates were recovered and columns were regenerated by treatment with 10 mL of 50 mM sodium citrate, pH 5.9. Data were corrected for full recovery of radioactivity, which ranged from 75 to 100%.

Calculations of Equilibrium Constants. Calculations are based on the molecular weight of 90 000 for monomeric R1, as predicted from the gene sequence (*18*). The equilibrium constants evaluated in this work are defined in Table 1 (see also Scheme 1), in which L refers to allosteric effector (dTTP or dGTP), S refers to substrate (GDP or ADP), and C refers to the $R1_2R2_2$ complex.

Calculations Based on Dynamic Light-Scattering Data. The dependence of measured molecular mass of R1, W, on allosteric effector (dTTP or dGTP) concentration is given by eq 1, derived from Scheme 1, in which it is assumed that both equivalents of effector bind with the same intrinsic dissociation constant K_L.

$$W = \{M[R1]/[R1]_t\}\{\{(K'_L + [L])/K'_L\} + \{4[R1](K_L + [L])^2/K_o K_L^{\,2}\}\} \qquad (1)$$

Scheme 1: Ligand Binding to mR1[a]

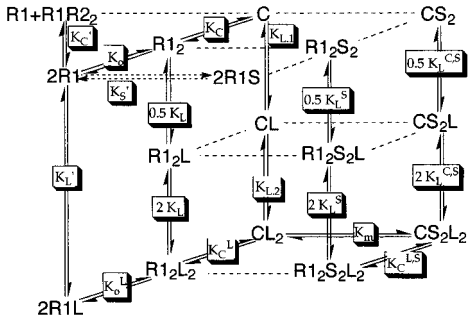

[a] Species are in bold-face type, equilibrium constants, defined in Table 1, are in plain text, experimentally determined parameters are represented by the equilibrium arrows, and the remaining parameters are represented by dashed lines. The value of K'_S depends on the results in Figure 1B and the derived constant K_S, and is therefore represented by dashed equilibrium arrows. C is the $R1_2R2_2$ complex.

In eq 1, M is the mass of monomer, $[R1]_t$ and $[L]_t$ are the total concentrations of enzyme (calculated as monomer) and effector added to solution, respectively and [R1] and [L] are calculated from eqs 1a and 1b, respectively. Best fit values for K_o, K_L, and K'_L were obtained using an iterative method.

$$[R1] = \{-X + \{X^2 + 8\,K_o K_L{}^2 (K'_L)^2 [R1]_t (K_L + [L])^2\}^{1/2}\}/4K'_L(K_L + [L])^2 \quad (1a)$$

where $X = K_o K_L{}^2 (K'_L + [L])$.

$$[L] = \{-Y + \{Y^2 + 8K_o K_L{}^2 (K'_L)^2 [L]_t [R1]^2\}^{1/2}\}/4K'_L[R1]^2 \quad (1b)$$

where $Y = K_L\{2K'_L[R1]^2 + K_o K_L (K'_L + [L]_t)\}$.

Specifically, for each measurement of W, [L] was initially set equal to $[L]_t$, and initial values of K_o, K_L, and K'_L were obtained by fitting the data to eqs 1 and 1a using Igor (Wavemetrics, Inc.). For each $[L]_t$, these initial parameter and [R1] values permitted calculation of a corrected [L] value, using eq 1b and SigmaPlot (Jandel Scientific). The corrected values of [L] were then reintroduced into eqs 1a and 1b, permitting recalculation of parameter and [R1] values. Iteration was continued until the calculated value of [L] changed by less than 1% between iterative cycles.

Equations 1, 1a, and 1b were also used to estimate apparent K_o, K_L, and K'_L values for effector-induced dimerization of R1 in the presence of substrate, GDP in the case of dTTP and ADP in the case of dGTP. $K^S_{o,app}$ is given by eq 1c, which can be rearranged to eq 1d, permitting evaluation of K'_S, when K_m, K^L_C, $K^{L,S}_C$, K_L, and K^S_L have been determined.

$$K^S_{o,app} = K_o\{1 + ([S]/K'_S)^2\}/\{1 + ([S]/K_S)^2\} \quad (1c)$$

$$K'_S = [S]/\{(K^S_{o,app}/K_o)^{1/2}(1 + [S]/K_S) - 1\} \quad (1d)$$

$$\text{where } K_S = (K_m K_L/K^S_L)(K^L_C/K^{L,S}_C)^{1/2} \quad (1e)$$

Calculations Based on Equilibrium Sedimentation Data. The apparent dissociation constant for $R1_2$ formation in the presence of the allosteric activator, L, is given by eq 2.

$$K^L_{o,app} = [R1]_t{}^2/[R1_2]_t = K_o(1 + [L]/K'_L)^2/(1 + [L]/K_L)^2 \quad (2)$$

Measurement of $K^L_{o,app}$ at two different [L] values, $[L_a]$ and $[L_b]$ over a range in which $[L] \gg K_L$, $[R1]_t$ permits estimation of K'_L from eq 2a

$$K'_L = [L_a][L_b](r^{1/2} - 1)/([L_b] - r^{1/2}[L_a]) \quad (2a)$$

where $r = K^{L,a}_{o,app}/K^{L,b}_{o,app}$

Calculations Based on Effector Binding Assay Data. The concentration of bound effector was calculated as the difference between the total and filtrate effector concentrations. Effector binding data was fit by Igor to the Scatchard-type eq 3 derived from Scheme 1, yielding estimates for $K^C_{L.1}$ and $K^C_{L.2}$. In these equations, ν is the number of equivalents of effector bound per $R1_2$, and n is equal to 2.

$$\nu/[L] = \{K^C_{L.2}(n - \nu) + \{(K^C_{L.2}(n - \nu))^2 + 4K^C_{L.1}K^C_{L.2}\nu(2n - \nu)\}^{1/2}\}/2K^C_{L.1}K^C_{L.2} \quad (3)$$

Calculations Based on GDP and ADP Reductase Data. All velocity measurements were carried out in the presence of excess R2 over R1, under conditions in which virtually all R1 is present as the $R1_2R2_2$ complex, C. The velocity of substrate reduction as a function of increasing substrate concentration in the presence of saturating effector concentration was fit with the normal Michaelis−Menten eq 4, yielding estimates of K_m and k_{cat}. Here, $[R1]_t$ is the total concentration of R1 added to solution, calculated as monomers. At low $[S]_t$, [S] is calculated from eq 4a, which is derived assuming that K_m is the dissociation constant for S binding to the enzyme. The justification for this assumption is the very slow turnover of S.

$$\upsilon = k_{cat}[R1]_t[S]/(K_m + [S]) \quad (4)$$

$$[S] = 0.5\{[S]_t - ([R1]_t + K_m) + \{([R1]_t + K_m - [S]_t)^2 + 4K_m[S]_t\}^{1/2}\} \quad (4a)$$

The velocity of substrate reduction as a function of increasing effector concentration at saturating [S] was fit with eq 5 derived from Scheme 1 where $K^{C,S}_L$ represents the

$$\upsilon = [L](2K^{C,S}_L V_1 + [L]V_2)/(K^{C,S}_L + [L])^2 \quad (5)$$

intrinsic dissociation constant of effector ligand from the CS_2 complex (i.e., effector binding is assumed noncooperative), V_1 represents the velocity of substrate reduction by the complex with one effector bound, and V_2 represents the velocity of substrate reduction by the complex with two effectors bound. The concentration of effector L is given by eq 5a, in which $[CS_2]_t$ is equal to the total concentration of R1 added to solution, calculated as dimers, by close analogy with eq 4a.

$$[L] = 0.5\{[L]_t - (2[CS_2]_t + K^{C,S}_L) + \{(2[CS_2]_t + K^{C,S}_L - [L]_t)^2 + 4K^{C,S}_L[L]_t\}^{1/2}\} \quad (5a)$$

The dependence of dTTP-activated GDP reductase on $R2_2$ concentration at fixed R1 concentration and near-saturating concentrations of both dTTP and GDP is given by eq 6

$$\upsilon = V[C]_t/[R1_2]_t \quad (6)$$

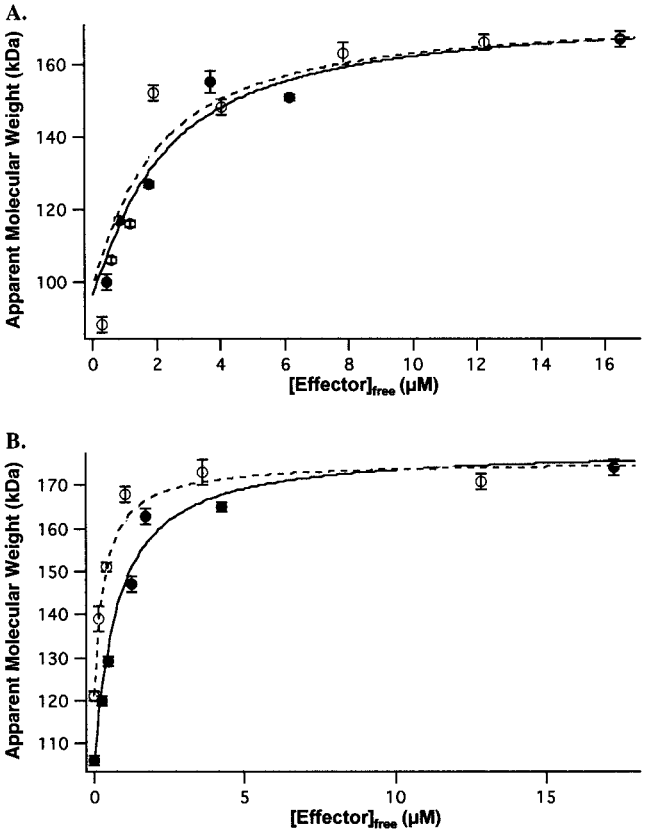

FIGURE 1: Dependence of R1 molecular mass on allosteric effector concentration, as measured by dynamic light scattering. Solid and dashed lines show best fits of dGTP and dTTP data, respectively, to eq 1. (A) Absence of substrate. Solutions contained varying dGTP and R1 (7.6 μM) (●) or varying dTTP and R1 (7.6 μM) (○) in buffer B. Data are reported as average ± standard deviation (12 determinations per point). (B) At saturating substrate. Solutions contained varying dGTP, ADP (0.37 mM), and 6.1 μM R1 (●) or varying dTTP, GDP (1 mM), and R1 (7.0 μM) (○) in buffer B. Data are reported as average ± standard deviation (≥10 determinations per point). R1 concentrations are calculated as monomer.

in which $[C]_t$ is given by eq 6a, and V is the velocity at saturating $[R2_2]$:

$$[C]_t = 0.5\{([R1_2]_t + [R2_2]_t + K_C^{L,S}) + \{([R2_2]_t + K_C^{L,S} - [R1_2]_t)^2 + 4K_C^{L,S}[R1_2]_t\}^{1/2}\} \quad (6a)$$

The dependence of dTTP-activated GDP reductase on the addition of dGTP (G) to a solution in which both specificity sites in CS_2 are filled with dTTP (T) was fit with eq 7,

$$v = K_G^{C,S}[T]\{V_1K_G^{C,S}[T] + 2V_2K_T^{C,S}[G]\}/\{K_G^{C,S}[T] + K_T^{C,S}[G]\}^2 \quad (7)$$

where $K_T^{C,S}$ and $K_G^{C,S}$ are the intrinsic dissociation constants for the binding of dTTP and dGTP to CS_2 (where S is GDP), respectively, and V_1 and V_2 are the velocities of GDP reduction from the $CS_2(dTTP)_2$ and CS_2dTTPdGTP complexes, respectively. All effector binding is assumed to be noncooperative.

Calculations Based on Biosensor Data. R1 binding to an R2 biosensor allows measurement of the amount of R1 bound as a function of R1 in solution. Published data of others (*32*) were fit to eq 8 for binding experiments carried out in the absence of effector, allowing estimation of K_C and K'_C, using the value for K_o determined from light-scattering studies. They were also fit to eq 9 for binding experiments carried out in the presence of saturating dTTP or dGTP, where $[R1]_t$ is equal to $2[R1_2L_2]$, permitting evaluation of K_C^L. In these equations, ν is the number of R1 monomers bound per R2 dimer.

$$\nu = [R1](K_oK_C + 2K'_C[R1])/(K_oK_CK'_C + K_oK_C[R1] + K'_C[R1]^2) \quad (8)$$

$$\nu = 2[R1_2L_2]/(K_C^L + [R1_2L_2]) \quad (9)$$

Table 2: Parameter Values[a]

parameter	S = GDP, L = dTTP	S = ADP, L = dGTP	relevant figure	relevant equation
K_o	150 ± 30	180 ± 120	1A	1
K'_S	119 ± 95	nd[b]	1B[c]	1d
K_S	36 ± 28	nd	derived constant[d]	
K_o^S	15 ± 12	nd	derived constant[e]	
K'_L	25 ±17 (DLS)[f]	33 ± 12 (DLS)	1A	1
	37 ± 13 (SE)[g]		3	2a
K_L	0.55 ± 0.25	0.5 ± 0.3	1A	1
	0.3	**0.25**		
K_L^S	0.20 ± 0.08	0.30 ± 0.14	1B	1
$K_{L.1}^C$	3.2 ± 0.7	1.5 ± 0.3	4	3
	3.9	**1.7**		
$K_{L.2}^C$	0.6 ± 0.2	1.0 ± 0.2	4	3
	0.8	**1.1**		
K_m	4.9 ± 0.6	12 ± 1	5	4
$K_L^{C,S}$	1.26 ± 0.07[h]	0.7 ± 0.1[h]	6	5
	(0.59 ± 0.04)[i]	(0.36 ± 0.06)[i]		
$K_C^{L,S}$	0.021 ± 0.014	nd	7	6
K_C	0.011 ± 0.004		9	8
	0.015			
K'_C	>5 μM		9	8
K_C^L	0.8 ± 0.3	0.6 ± 0.2	9	9
	0.5	**0.45**		
k_{cat} (s^{-1})	0.28 ± 0.01	0.18 ± 0.01	5	4
	0.27 ± 0.04	0.23 ± 0.01	6	5

[a] All dissociation constants are μM. Bolded values are demanded by thermodynamics (see text). [b] nd, not determined. [c] The value of K'_S depends in Figure 1B and the derived constant K_S (see text). [d] $K_S = (K_mK_L/K_L^S)(K_C^L/K_C^{L,S})^{1/2}$. [e] $K_o^S = K_o(K_S/K'_S)^2$. [f] DLS, dynamic light scattering. [g] SE, sedimentation equilibrium. [h] Cooperative case (see text). [i] Noncooperative case (see text).

RESULTS

Effector- and Substrate-Induced Dimerization of mR1. In the absence of ligands, the apparent molecular mass of R1, as determined by dynamic light scattering (90−100 kDa, Figure 1A) is consistent with most of the protein being monomeric. This conclusion is also consistent with the sedimentation constant of 6.9 S, determined by sedimentation velocity (Figure 2), versus a calculated *s* value of 6.4 for a monomer of mass 90 kDa, assuming a spherical shape (equation I). The higher measured value of s may reflect the presence of a small amount of R1 dimer ($R1_2$). Addition of either dTTP or dGTP promotes the formation of $R1_2$, of apparent mass ~180 kDa (Figure 1A). Fits of the data in Figure 1A to eqs 1, 1a, and 1b give the values summarized in Table 2 for K_o, the apparent dissociation constant for R1

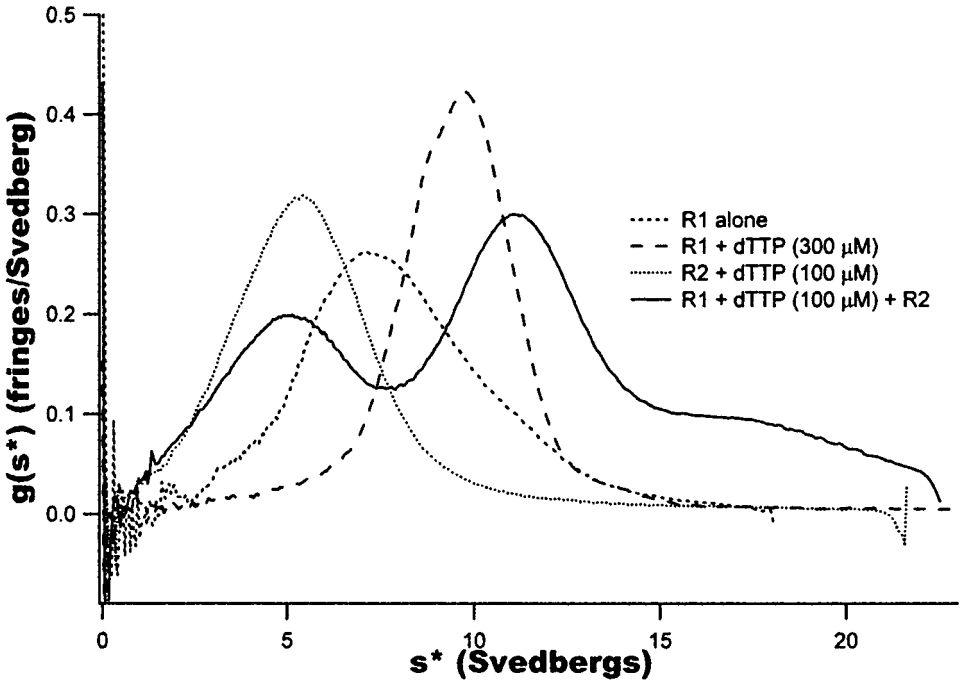

FIGURE 2: Sedimentation velocity experiments. (- - -) R1 alone; (— —) R1 + dTTP (300 μM); (•••) $R2_2$ (6 μM) + dTTP (100 μM); (——) R1 + dTTP (100 μM) + $R2_2$ (6 μM). In all experiments, R1 monomer was added at 7.8 μM.

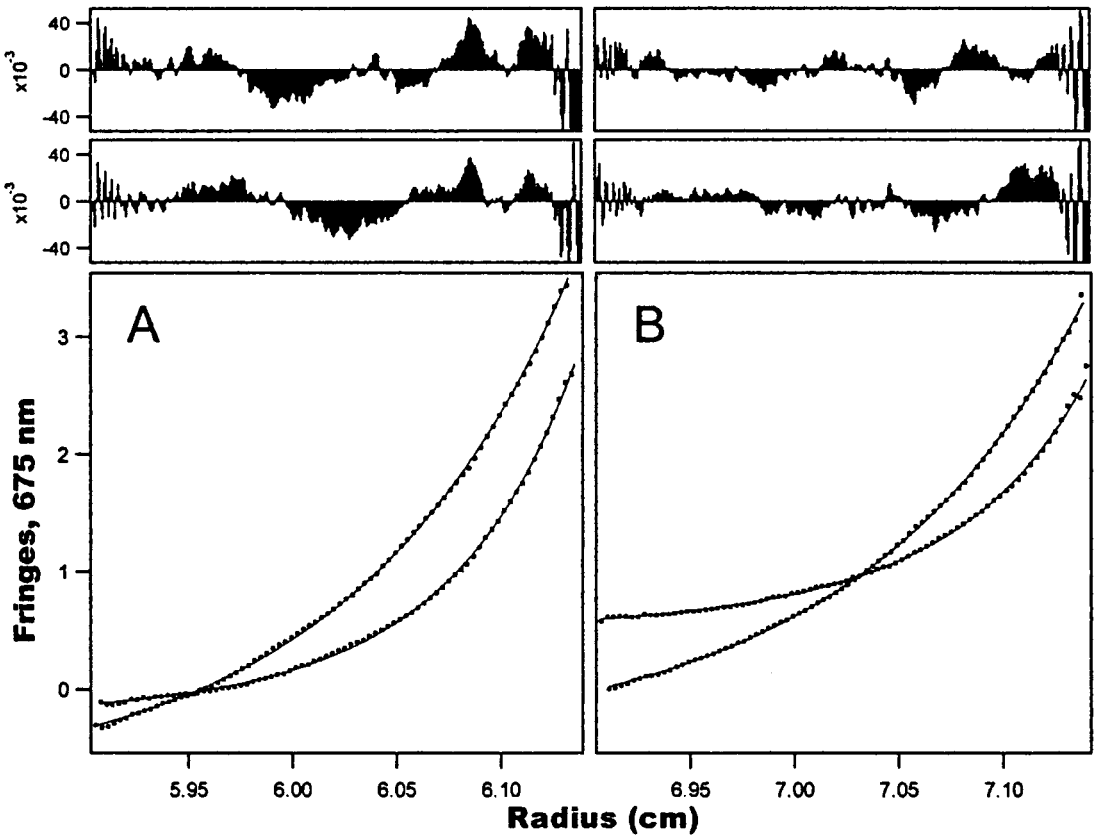

FIGURE 3: Sedimentation equilibrium experiments. R1 (7.8 μM monomer) + dTTP at 50 μM (A) or 300 μM (B). Shown are data fit to eq II and residuals from experiments at 8000 rpm (top) and 12 000 rpm (bottom), describing an equilibrium mixture of R1 and $R1_2$.

dimerization, and for K_L' and K_L, the apparent intrinsic dissociation constants for one-site binding to R1 and two-site binding to $R1_2$, respectively, of either dTTP or dGTP. Much poorer fits were obtained to a model allowing only 1 equiv of effector to bind to $R1_2$ (data not shown). Interestingly, both effectors have, within experimental error, identical affinities for R1.

Sedimentation velocity experiments also demonstrate dTTP induction of R1 dimerization as addition of 300 μM dTTP increases the measured *s* value of R1 from 6.9 to 9.9 S (Figure 2). The calculated *s* value for a spherical particle with a mass of 180 kDa is 10.1 S. Sedimentation equilibrium experiments with R1 in the presence of either 50 or 300 μM dTTP permit calculation of apparent dimerization dissociation

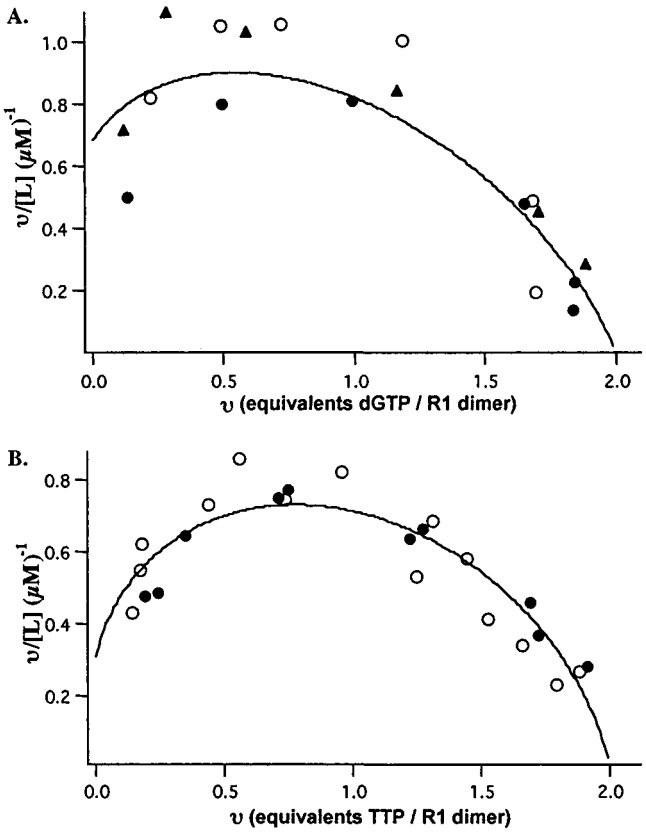

FIGURE 4: Binding of effectors to complex C. (A) dGTP binding. Assay mixtures contained 1.9 μM $R1_2$ and 9.6 μM $R2_2$ (○), 2.9 μM $R1_2$ and 14.5 μM $R2_2$ (●), or 3.6 μM $R1_2$ and 12 μM $R2_2$ (▲). (B) dTTP binding. Assay mixtures contained 1.9 μM $R1_2$ and 9.4 μM $R2_2$ (○) or 2.9 μM $R1_2$ and 14.8 μM $R2_2$ (●). All binding assays were conducted in buffer B with 50 μM $FeCl_3$ and effector concentrations ranging from 0.5 to 18 μM. Binding measurements were made after a five minute incubation at 25 °C. Data are fit to eq 3. Each point is the average of duplicate measurements. Actual extrapolated stoichiometries were 1.7/$R1_2$ and 1.6/$R1_2$ for dTTP, and dGTP, respectively. These were adjusted to 2.0, assuming that the active R1 concentration was overestimated.

constants of $10^{-5.72 \pm 0.02}$ and $10^{-6.11 \pm 0.04}$, respectively (Figure 3), and enable estimation of K'_L from eq 2a. As is clear from Table 2, the value of K'_L determined by sedimentation equilibrium is identical within experimental uncertainty to that determined from light-scattering measurements.

Both purine substrates also promote dimer formation. Comparison of panels A and B of Figure 1 shows that the apparent molecular mass of R1 increases on addition of either ADP or GDP, and that, in the presence of each of these substrates, the effector concentration required to induce R1 dimerization is reduced. Fitting the data in Figure 1B to eqs 1, 1a, and 1b provides estimates of apparent K_o and K_L values in the presence of the activated substrate, GDP by dTTP and ADP by dGTP. The apparent K_L values are little changed in the presence of the saturating substrate concentrations employed (vide infra), so that it is clear that K_L is about equal to K_L^S for both the dTTP-dGDP and dGTP-ADP pairs. The $K^S_{o,app}$ value allows estimation of K'_S from eq 1d, using the K_o value determined above, and the value for K_S derived knowing other constants in Scheme 1 (eq 1e). Summarizing, purine substrates directly promote dimer formation ($K_o > K_o^S$) by binding more tightly to R1 dimer than to R1 monomer ($K'_S > K_S$) but exert little influence on effector binding to dimer ($K_L \approx K_L^S$).

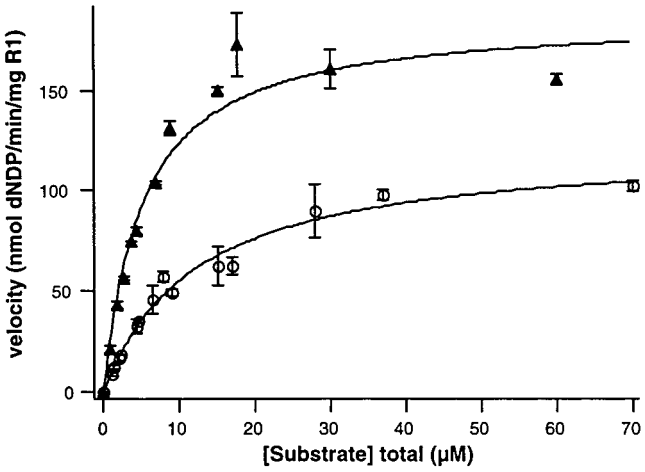

FIGURE 5: Purine reductase activity versus substrate concentration. Assay mixtures contained 1.2 μM R1, 2 μM $R2_2$, and 330 μM effector in buffer B plus 50 μM $FeCl_3$ with ADP (○) and GDP (▲) concentrations shown. Measurements were made at 25 °C under initial rate conditions. Data are fit to eq 4. Each point is the average of duplicate measurements ± average deviation.

R2 Binding to R1. Analytical sedimentation velocity experiments provide clear evidence that R1 dimer forms a complex with R2 dimer, $R1_2R2_2$ (denoted C). Thus, adding $R2_2$ (*s* value, 5.4 S) to $R1_2$, formed by addition of 100 μM dTTP, increases the *s* value from 9.9 to 11.5 S (Figure 2). This value may reflect incomplete formation of the complex in solution, as the calculated *s* value for a spherical mass of 270 kDa, corresponding to C, is 13.2 S. Significant deviation of the shape of C from spherical would also decrease its *s* value. Similarly, the deviation of the measured *s* value of $R2_2$ (5.4 S) from its predicted value assuming a spherical shape (6.4 S) indicates either some dissociation of $R2_2$ to monomer, deviation from a spherical shape, or both. Quantitative estimates of the dissociation constant for $R1_2$ binding to $R2_2$ in the presence or absence of substrate and/or effector are presented below.

Cooperative Effector Binding to the R1−R2 Complex. Experiments performed at protein concentrations such that virtually all of the R1 is present in complex C (see Discussion) show that binding of either dTTP or dGTP is highly cooperative (Figure 4) and proceeds with a stoichiometry of 2 ligands per R1 dimer (see Figure 4 legend). Fits of the data to eq 3 give dissociation constant values of 3.2 ± 0.5 and 0.6 ± 0.1 μM for binding the first and second equivalents of dTTP, respectively, with a Hill *n* of 1.6. The corresponding values for dGTP are 1.5 ± 0.1 and 1.02 ± 0.02 μM, with a Hill *n* of 1.4. After correction for statistical factors, these values correspond to increases in the apparent affinity of the second equivalent of 6−20-fold vs the first equivalent. It is noteworthy that this cooperativity is essentially independent of protein concentration, i.e., it reflects cooperative binding to $R1_2R2_2$, rather than being linked to R1 dimerization or to complex formation between $R1_2$ and $R2_2$.

Purine Reductase Activity. Under conditions in which the large majority of R1 in solution is present as effector-saturated C complex prior to the addition of substrate, both GDP and ADP reductase activities follow a simple Michaelis−Menten model (Figure 5), giving the K_m and k_{cat} values collected in Table 2. The value of k_{cat} (0.28 s^{-1}) corresponds

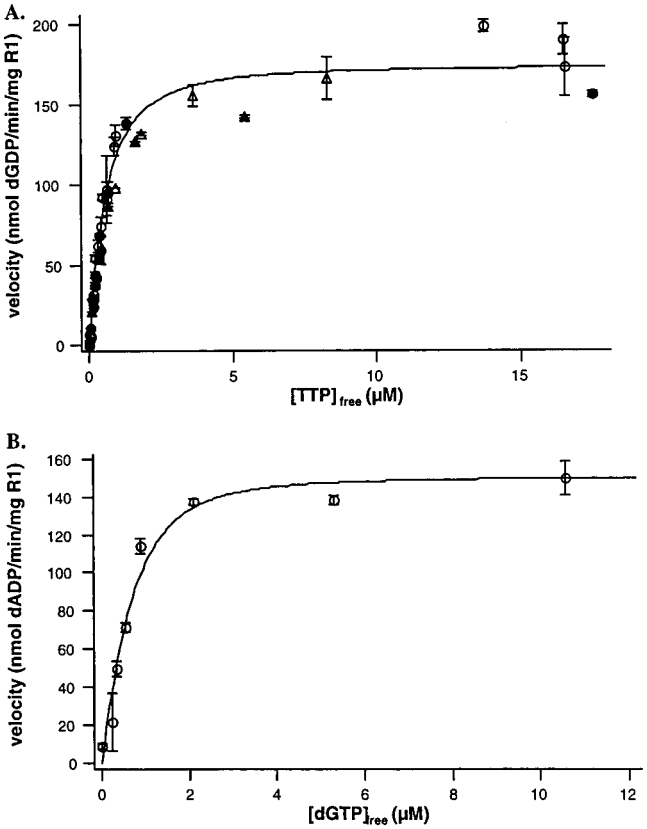

FIGURE 6: Purine reductase activity versus effector concentration. Assay mixtures contained (A) 1 mM GDP, dTTP as shown, and either 1 μM R1 and 2.3 μM $R2_2$ (●), 2 μM R1 and 4.6 μM $R2_2$ (○), 4.1 μM R1 and 8.7 μM $R2_2$ (Δ), or 5.9 μM R1 and 13.1 μM $R2_2$ (▲). (B) 350 μM ADP, 0.5 μM R1, 3.2 μM $R2_2$, and dGTP as shown. Data are fit (solid lines) to eq 5, with V_1 equal to V_2 (cooperative model; see text). Assays were performed in buffer B at 25 °C under initial rate conditions. Each point is the average of duplicate measurements ± average deviation.

to a specific activity of 190 nmol/mg of R1/min. This is the highest value reported for mammalian R1 (see, for example, refs *20*, *22*, and 33) and is comparable to the value reported for the reduction of CDP by *Escherichia coli* R1 when DTT is the external reductant (118 nmol/mg of R1/min, ref *34*).

In the absence of allosteric effector both reductase activities are essentially nil, even at substrate concentrations >100-fold the K_m values determined above. The dependence of reductase activity on effector concentration (Figure 6) allows estimation of apparent dissociation constants $K_L^{C,S}$ for dTTP and dGTP from substrate-saturated $R1_2R2_2$ complexes. The fitted values of these constants depend on whether it is assumed that full activity is conferred by the binding of a single effector molecule per dimer (the cooperative case) or whether half of the full activity is conferred for the binding of each effector molecule per dimer (the noncooperative case) (Table 2). Both sets of data are fit better by the cooperative case (see also below), yielding values of 1.26 ± 0.07 μM for dTTP and 0.7 ± 0.1 μM for dGTP. The corresponding values for the noncooperative case are 0.59 ± 0.04 and 0.36 ± 0.06 μM, respectively.

That the dTTP dependence of the specific activity of GDP reduction displays little or no change with increasing protein concentration (Figure 6) is strong evidence that virtually all R1 is present as $R1_2R2_2$ complex throughout the titration. Confirmation of this point is provided by results measuring

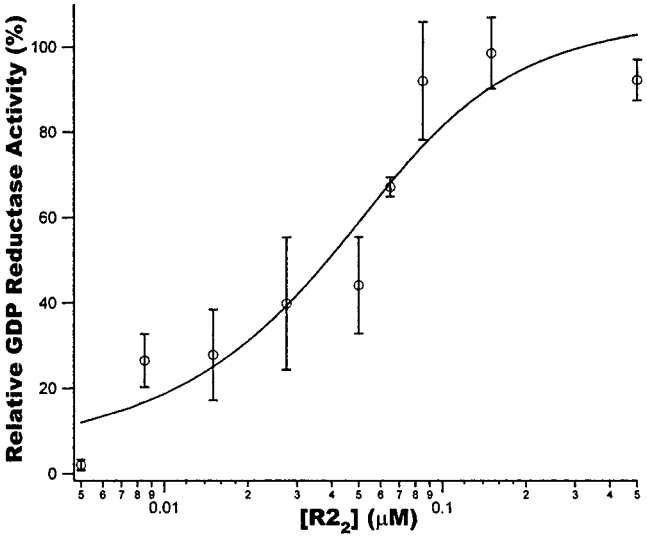

FIGURE 7: GDP reductase versus $R2_2$ concentration. Semilogarithmic plot. Assay mixtures contained 0.1 μM R1, 30 μM GDP, and 300 μM dTTP in buffer B plus 50 μM $FeCl_3$ with $R2_2$ concentrations shown. Measurements were made at 25 °C under initial rate conditions. Data are fit to eq 6. Each point is the average of 2−8 measurements ± average deviation.

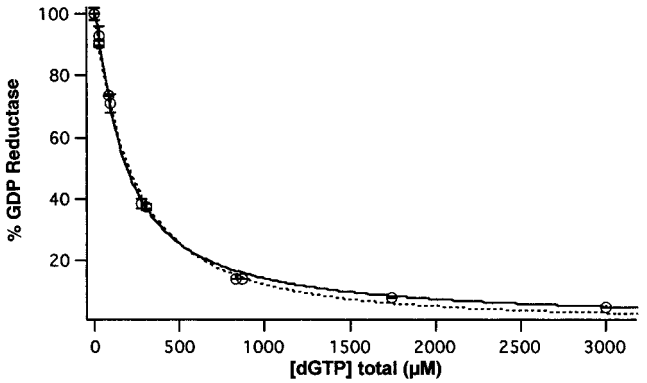

FIGURE 8: GDP reductase versus dGTP concentration at 100 μM dTTP. Assay mixtures contained 1.9 μM R1, 10.7 μM $R2_2$, and 85 μM dTTP in buffer B with dGTP concentrations shown. Measurements were made at 25 °C under initial rate conditions. Data are fit to eq 7 with the specific activity of the mixed state equal to 100% (solid line) or 1.8% (dashed line) the activity of the dTTP saturated enzyme. Data are reported as the average of duplicate measurements ± average deviation.

the dependence of GDP reductase on $R2_2$ concentration (Figure 7), which permit estimation of the apparent dissociation constant $K_C^{L,S}$ for $R2_2$ binding to $R1_2$ (Table 2).

Interestingly, while the extrapolated maximum velocity for GDP reduction at saturating GDP and dTTP is the same in Figures 5 and 6, the extrapolated maximum velocity of ADP reduction at saturating ADP and dGTP concentrations is about 25% lower in Figure 5 than in Figure 6 (Table 2). This discrepancy is not fully understood and may reflect both the tendency of adenine nucleotides to favor aggregation of R1 (O.B.K. et al., in preparation) and the differences in protein and ADP concentrations employed in these two experiments.

While both dTTP and dGTP promote R1 dimerization, only dTTP activates reduction of GDP. By contrast, dGTP inhibits dTTP-activated GDP reduction (Figure 8), consistent with competition between dGTP and dTTP for binding to the specificity site. The two limiting assumptions for the

cooperative case, which yield equivalent fits, are that the mixed state ($R1_2R2_2$dTTP·dGTP) is either fully active or fully inactive. These assumptions give calculated values for the intrinsic dissociation constant of dGTP from the GDP-saturated enzyme−cofactor complex of 1.24 ± 0.09 or 6.7 ± 0.5 μM, respectively. Thus, the assumption that dGTP binding to form the mixed state has no effect on GDP reductase yields a dissociation constant for dGTP binding quite similar to that for the ADP-saturated enzyme, whereas the contrary assumption that dGTP binding inhibits GDP reductase in the mixed state results in a considerably larger dissociation constant for dGTP binding to the ADP-saturated enzyme. For the noncooperative case, in which the mixed state is half-active, the calculated dissociation constant to the ADP-saturated enzyme is 1.32 ± 0.08 μM, but the fit is much poorer. That the fits to the data in both Figures 6 and 8 are much better for the cooperative case leads us to conclude that the cooperative case is a more accurate representation of RR activity.

DISCUSSION

Quantitative Model for Purine Diphosphate Reductase Activity. ADP and GDP reductase activities are functions of R1, R2, substrate (S), and allosteric effector (L) concentrations. The model in Scheme 1 presents for the first time a fully quantitative treatment of these activities, specifically considering the dimerization of R1 and the differential affinities that ligands have for monomeric and dimeric R1. Scheme 1 accounts quantitatively not only for the results presented in this paper, but also for related results of ourselves and others (see below). It has several points in common with results for the murine enzyme recently published by Reichard et al. (*33*) that supplant earlier work (*14*). These points include two effector binding sites per R1 dimer (Figure 4), the numerical value of K_L for dGTP (0.56 μM at 25 °C, Table 2, vs 0.2 μM at 4 °C in ref *33*), and one $R2_2$ bound per $R1_2$ [Figure 2, see also the docked structure proposed for the *E. coli* $R1_2R2_2$ complex (*35*)]. Scheme 1 also posits a substrate stoichiometry of 2/dimer, by analogy with the results of single turnover experiments on the *E. coli* dimer (*36*).

As presented, the model involves a total of 16 forms of R1, and its exact solution requires, at a minimum, experimental determination of 15 independent parameters. In fact, a total of 16 determined parameters are presented in Table 2, of which 13 were estimated from results presented above and three were estimated by fitting published results of others to expressions derived from Scheme 1. Eight parameters were estimated for each substrate−activator set (GDP−dTTP, ADP−dGTP) by four titrations involving measurements of two-site activator binding to R1 dimer, either as $R1_2$, $R1_2S_2$ [both via dynamic light scattering (DLS)], $R1_2R2_2$ (direct binding), or $R1_2R2_2S_2$ (activity studies). The first, second and fourth of these titrations were fit assuming noncooperative binding, so that both binding events could be described by an intrinsic constant and the appropriate statistical factor of 2 for the first dissociation and $^1/_2$ for the second. Noncooperative dGTP binding to $R1_2$ has recently been reported by Reichard et al. (*33*). While it is possible that effector binding to either $R1_2S_2$ or CS_2 is cooperative, the measurements used to evaluate such binding (molecular weight and enzyme activity) did not permit distinction between cooperative and noncooperative binding. By parsimony, noncooperative binding was assumed for these interactions. In summary, effector binding to all four forms of $R1_2$ is described by a total of five dissociation constants K_L, K_L^S, $K_{L.1}^C$ and $K_{L.2}^C$, and $K_L^{C,S}$.

Two parameters measuring substrate binding, K_s' and K_m, are provided by analysis of the influence of substrate on effector binding, measured by DLS and by the dependence of activity on substrate concentration, respectively. DLS measurements also allow estimation of K_o, and DLS and sedimentation equilibrium experiments provide a measure of K_L'. The 13th parameter measured above is $K_C^{L,S}$, obtained by measuring RR activity as a function of [$R2_2$]. The final three parameters, K_C, K_C', and K_C^L come from fitting the data of Ingemarson and Thelander (*32*), reproduced in Figure 9, to eqs 8 and 9. These workers used surface plasmon resonance to measure mR1 binding to dimeric R2 covalently bound to a sensor chip in the presence or absence of either dTTP or dGTP. Their data show that R1 binding is cooperative in the absence of added specificity site ligands and noncooperative in their presence, reflecting the much weaker binding of monomeric vs dimeric R1 to immobilized $R2_2$, and the shift of R1 from predominantly monomer in the absence of effectors to predominantly dimer in their presence. A summary of the relevant equations and figures used in evaluating the 16 parameters is presented in Table 2.

Since one additional parameter is measured than is needed to determine the 16 species in Scheme 1, the system is slightly overdetermined, specifically for the thermodynamic square connecting the species $R1_2$, C, $R1_2L$, $R1_2L_2$, CL, and CL_2. Consideration of the values obtained with those required by thermodynamics provides important insight into the limitations of the precision with which some of the parameters are determined and the importance of the error limits presented in Table 2. By thermodynamics, $(K_L)^2K_C^L$ must equal $K_{L.1}K_{L.2}K_C$, yet using the values listed in Table 2 for dTTP, and ignoring the error ranges, the first and second terms are equal to 0.25 and 0.020 μM^3, respectively. However, both terms can be set equal to 0.047 μM^3, using parameter values falling within the allowed error ranges, shown in bold in Table 2. An identical argument can be presented for parameters measured in the presence of dGTP, for which the common value of the parameter products is 0.028 μM^3.

Significance of the Parameters. The values of the parameters in Table 2 are important for understanding the effects of R1 ligands on R1 dimerization, identifying both homotropic and heterotropic binding effects, and for examining the quantitative effects of allosteric ligands on activity. Below we examine each of these issues in turn.

R1 Dimerization. Our finding that mR1 is predominantly a monomer in the absence of added ligands agrees with earlier results showing purified mammalian R1 from various sources to be monomeric (*14*, *37*). The value of the dissociation constant for dimer formation (K_o, 165 μM), determined for the first time in this work, is vastly in excess of any plausible in vivo concentration and indicates how little dimer formation takes place in the absence of ligands. This behavior is in marked contrast to *E. coli* R1, for which the dimeric state is the dominant form in solution even in the absence of ligands (*15*). On the other hand, each of the three

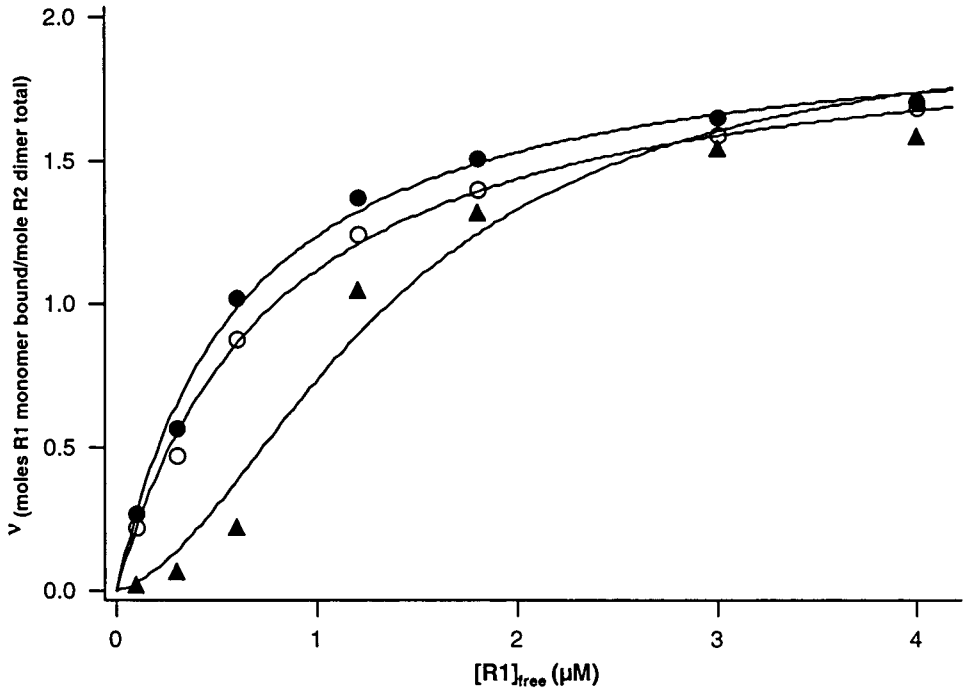

FIGURE 9: R1 binding to biosensor-immobilized R2 in the absence or presence of effector. Data from Ingemarson and Thelander (*32*) fit to eq 8 [absence of effector (▲)] or eq 9 [presence of saturating (100 μM) dTTP (○) or dGTP (●)]. Actual extrapolated stoichiometries were 1.45 R1/$R2_2$ in the absence of effector and 1.8 R1/$R2_2$ in the presence of effector. Data were adjusted to extrapolated stoichiometries of 2.0, assuming that the active $R2_2$ concentration was overestimated.

ligand types for R1 investigated in this work (allosteric effectors, substrates, and $R2_2$) favor $R1_2$ formation. Both dTTP and dGTP show very large effects, binding (on average) approximately 50 times more tightly to each dimer specificity site than to the corresponding site on monomer. Such large effects are in accord with structural studies on *E. coli* R1, placing the specificity site at the dimer subunit: subunit interface (*38*). By contrast, the GDP effect is more modest, with binding to the dimer only ~3 times tighter than to monomer.

R2 contacts R1 principally, if not exclusively, via the C-terminal heptapeptide of R2 (*17*, *19*). The lower limit estimate of K'_c, ≥ 5 μM, for R1 monomer binding to $R2_2$, while poorly determined, is clearly of the right order of magnitude, being quite similar to the value obtained for the binding of the *N*-acetylated form of the C-terminal peptide itself (~10 μM) and the values of 6−18 μM obtained for the interaction of either a single *E. coli* R2 C-terminus or a C-terminal *E. coli* R2 peptide with *E. coli* $R1_2$ (*39*, *40*). The $\geq$500-fold tighter binding (K'_c/K_c) of $R2_2$ to $R1_2$ than to R1 monomer may be plausibly attributed to a chelating effect when two such interactions are involved.

Heterotropic and Homotropic Cooperativity in Effector, Substrate, and R2 Dimer Binding and RR Activity. Of the three pairwise heterotropic interactions for the $R1_2$ ligands allosteric effector, substrate, and $R2_2$, the two involving $R2_2$ are opposite in their effects. Allosteric effector has a negative effect on $R2_2$ binding, whether measured as the ratio of K_C^L to K_C (~35) or $K_C^{L,S}$ to K_C^S (~40). Substrate, on the other hand, has a strongly positive effect, measured as the ratio of K_C^S to K_C (~0.035) or $K_C^{L,S}$ to K_C^L (~0.04). The two effects are opposite and almost equal, as seen by the similarity in the values of K_C and $K_C^{L,S}$.

Heterotropic cooperativity in $R2_2$, substrate, and effector binding recalls the work of Karlsson et al. (*41*), demonstrating that effector and substrate binding influence the rate of R2 inactivation by hydroxyurea within *E. coli* RR. Allosteric effects on RR activity have usually been thought of in terms of sites within R1. However, the differing effects of $R2_2$ on substrate and allosteric ligand binding shown in this work, and the influence of nucleotide effectors and substrates on the lability of the tyrosyl radical shown in ref *41*, clearly indicate that $R2_2$ both contributes and responds to the allosteric transition.

Other workers have observed apparent positive cooperativity between RR substrates and effectors (*42*, *43*). Here we clearly show for mammalian RR that the marked apparent positive heterotropic cooperativity between substrate and allosteric effector is principally an artifact of the synergistic influence of both of these ligands on the quaternary structure of R1. When associative cooperativity is eliminated by studying the binding of nucleotide ligands to the R1 dimer, the heterotropic effect between substrate and effector is only weakly positive, whether measured as the ratio of K_m to K_S^C (~0.25−0.50) or K_S^L to K_S (~0.5). This weak effect is in marked contrast to the dramatic dependence of reductase activity on the presence of the appropriate allosteric activator. Both GDP and ADP reductase activities are increased at least 100-fold in the presence of saturating dTTP and dGTP, respectively. As is clear from Scheme 1 and Table 2, both dTTP and dGTP bind to the specificity site with almost identical affinities and show almost identical selectivity for R1 dimer over monomer. A comparable statement can be made for the active site binding of GDP and ADP. Thus, although neither the specificity nor the active site displays nucleotide base specificity, as measured by binding affinity, RR activity depends almost entirely on specific pairwise interactions between the specificity and active sites (see, for example, Figure 8). As pointed out earlier by Mazat et al. (*44*), and now confirmed by the present work, the activation

resulting from these interactions arises primarily from effects on V_{max} rather than from effects on substrate binding.

Earlier workers have suggested the pairwise specificity represents a through-protein interaction between the specificity and active sites (*7*, *13*, *42*, *43*), consistent with the proximal placement of these two sites found more recently in the X-ray crystal structure of *E. coli* R1 (38). The homotropic positive cooperativity displayed by both dTTP and dGTP in their binding to $R1_2R2_2$ (Figure 4), which is independent of effects on R1 dimerization or on $R2_2$ binding to $R1_2$, indicates that effector binding induces a conformational change. This is consistent with the location of the specificity site at the R1 dimer interface. The potential importance of this conformational change for substrate activation is suggested by our finding that activity data is better fit by a model in which a single equivalent of bound effector is sufficient for full activation of purine substrate reduction. It may thus be that the higher affinity state for effector binding corresponds to the high activity state for substrate reduction.

Significance for Physiological Regulation. Here we present the first clear evidence for homotropic cooperativity in effector binding for an RR from any source. Our data further suggest that a single equivalent of allosteric effector is sufficient for full enzymatic activity. In addition, we show that the susceptibility of dimeric mammalian R1 to dissociation gives the murine enzyme access to associative cooperativity as a mode of allosteric regulation. As a result, changes in the quaternary structure of mammalian R1 must be explicitly considered in models accounting for its catalytic and regulatory function. It may be that evolution has endowed mammalian RR with such a broad array of regulatory controls because of the stringent demands made on its physiological function. This cytoplasmic enzyme must rapidly and accurately respond to subtle changes in deoxyribonucleotide pools located primarily in the nucleus. The *E. coli* R1 dimer, which is in direct contact with cellular deoxyribonucleotide pools, is much less susceptible to dissociation (*15*), and so is unlikely to be regulated via associative cooperativity. Associative cooperativity may therefore be an evolutionary adaptation in RR that was necessitated by cellular compartmentalization.

ACKNOWLEDGMENT

We gratefully acknowledge the excellent technical assistance of Nora Zuño in several technical aspects of this work, Chris Hamann, and Melissa Henriksen Wrzeszczynska for providing mR2, and Preston Hensley for providing the macro program for Igor Pro.

REFERENCES

1. Jordan, A., and Reichard, P. (1998) *Annu Rev. Biochem. 67*, 71−98.
2. Szekeres, T., Fritzer-Szekeres, M., and Elford, H. L. (1997) *Crit. Rev. Clin. Lab. Sci. 34*, 503−528.
3. Robins, M. J. (1999) *Nucleosides Nucleotides 18*, 779−793.
4. Hui, Y. F., and Reitz, J. (1997) *Am J Health Syst Pharm. 54*, 162−170.
5. Larsson, A., and Reichard, P. (1966) *J. Biol. Chem. 241*, 2533−2539.
6. Larsson, A., and Reichard, P. (1966) *J. Biol. Chem. 241*, 2540−2549.
7. Eriksson, S., Thelander, L., and Akerman, M. (1979) *Biochemistry 18*, 2948−2952.
8. Chang, C. H., and Cheng, Y. C. (1979) *Cancer Res. 39*, 5087−5092.
9. Eriksson, S., and Sjoberg, B. M. (1989) in *Ribonucleotide Reductase*, pp 189−216, CRC Press, Boca Raton.
10. Stubbe, J., and van der Donk, W. A. (1995) *Chem. Biol. 2*, 793−801.
11. Sjoberg, B. M. (1997) *Struct. Bonding 88*, 139−173.
12. Thelander, L., and Reichard, P. (1979) *Annu. Rev. Biochem. 48*, 133−158.
13. Brown, N. C., and Reichard, P. (1969) *J. Mol. Biol. 46*, 39−55.
14. Thelander, L., Eriksson, S., and Akerman, M. (1980) *J. Biol. Chem. 255*, 7426−7432.
15. Brown, N. C., and Reichard, P. (1969) *J. Mol. Biol. 46*, 25−38.
16. Mann, G. J., Graslund, A., Ochiai, E., Ingemarson, R., and Thelander, L. (1991) *Biochemistry 30*, 1939−1947.
17. Hamann, C. S., Lentainge, S., Li, L.-S., Salem, J. S. Yang, F.-D., and Cooperman, B. S. (1998) *Protein Eng. 11*, 219−224.
18. Caras, I. W., Levinson, B. B., Fabry, M., Williams, S. R., and Martin, D. W. J. (1985) *J. Biol. Chem. 260*, 7015−7022.
19. Fisher, A., Yang, F. D., Rubin, H., and Cooperman, B. S. (1993) *J. Med. Chem. 36*, 3859−3862.
20. Salem, J. S., Scott, C. P., Li, L.-S., Cooperman, B. S., and Rubin, H. (1993) *FEBS Lett. 323*, 93−95.
21. Yang, F. D., Spanevello, R. A., Celiker, I., Hirschmann, R., Rubin, H., and Cooperman, B. S. (1990) *FEBS Lett. 272*, 61−64.
22. Davis, R., Thelander, M., Mann, G. J., Behravan, G., Soucy, F., Beaulieu, P., Lavallee, P., Graslund, A., and Thelander, L. (1994) *J. Biol. Chem. 269*, 23171−23176.
23. Voet, D., Gratzer, W. B., Cox, R. A., and Doty, P. (1963) *Biopolymers 1*, 193−208.
24. Reyes, P. (1972) *Anal. Biochem. 50*, 35−39.
25. Ormo, M., and Sjoberg, B. M. (1990) *Anal. Biochem. 189*, 138−141.
26. Stafford, W. F. (1992) *Anal. Biochem. 203*, 295−301.
27. Stafford, W. F. (1994) *Methods Enzymol. 240*, 478−501.
28. Stafford, W. F. (1997) *Curr. Opin. Biotech. 8*, 14−24.
29. Cantor, C. R., and Schimmel, P. R. (1980) *Biophysical Chemistry*, W. H. Freeman and Company, New York.
30. Brooks, I., Watts, D. G., Soneson, K. K., and Hensley, P. (1994) *Methods Enzymol. 240*, 459−478.
31. Laue, T. M. (1996) *Choosing Which Optical System of the Optima XL-I Analytical Ultracentrifuge to Use*, http://www.beckman.com/beckman/biorsrch/BioLit/Pubs/1821a(a).pdf, January 2001, Beckman Instruments, Inc., Fullerton, CA.
32. Ingemarson, R., and Thelander, L. (1996) *Biochemistry 35*, 8603−8609.
33. Reichard, P., Eliasson, R., Ingemarson, R., and Thelander, L. (2000) *J. Biol. Chem. 275*, 33021−33026.
34. Mao, S. S., Holler, T. P., Yu, G. X., Bollinger, J. M., Booker, S., Johnston, M. I., and Stubbe, J. (1992) *Biochemistry 31*, 9733−43.
35. Uhlin, U., and Eklund, H. (1994) *Nature 370*, 533−539.
36. Thelander, L. (1974) *J. Biol. Chem. 249*, 4858−4862.
37. Cory, J. G., Fleischer, A. E., and Munro, J. B. I. (1978) *J. Biol. Chem. 253*, 2898−2901.
38. Eriksson, M., Uhlin, U., Ramaswamy, S., Ekberg, M., Regnstrom, K., Sjöberg, B. M., and Eklund, H. (1997) *Structure 5*, 1077−1092.
39. Sjöberg, B.-M., Karlsson, M., and Jornvall, H. (1987) *J. Biol. Chem. 262*, 9736−9743.
40. Climent, I., Sjoberg, B. M., and Huang, C. Y. (1991) *Biochemistry 30*, 5164−5171.
41. Karlsson, M., Sahlin, M., and Sjoberg, B. M. (1992) *J. Biol. Chem. 267*, 12622−12626.
42. von Dobeln, U. (1977) *Biochemistry 16*, 4368−4671.
43. Eriksson, S. (1983) *J. Biol. Chem. 258*, 5674−5678.
44. Mazat, J. P., Langla, J., and Mazat, F. (1977) *J. Theor. Biol. 68*, 365−383.

BI002335Z